P-ISSN 1991-8941
E-ISSN 2706-6703
Vol. 20, No. 1 (2026)

Journal of University of Anbar for Pure Science
(JUAPS)

journal homepage: juaps.uoanbar.edu.iq

Open Access

Original Paper

Thermoelastic diffusion with dual-phase-lag: analysis of time-harmonic sources in a non-local framework

Rajneesh Kumar[1], **Pawan Kumari**[2*], **Menaka**[2]

[1]Department of Mathematics, Kurukshetra University, Kurukshetra 136119, India
[2]Department of Mathematics, Om Sterling Global University, Hisar. 125001, India

ARTICLE INFO

Received: 16/09/2025
Accepted: 07/12/2025
Available online: 16/03/2026
April Issue
10.37652/juaps.2025.165066.1681

Cite @ JUAPS

Corresponding author
Pawan Kumari
pawankumarigawarya@gmail.com

ABSTRACT

The present study is an investigation of the effects of non-locality and dual-phase-lags in a thermoelastic half-space subjected to thermomechanical loading. A homogeneous isotropic nonlocal thermoelastic diffusive half space with dual phase lag is explored. The governing equations are solved with the help of harmonic vibration analysis in collaboration with Fourier transform techniques. The distributed sources are considered to demonstrate practical relevance. Further, they are categorized as uniformly distributed sources and linearly distributed sources for mechanical, thermal, and chemical potential excitations. Numerical simulations are performed using software MATLAB (R2016a) to evaluate displacements, stresses, temperature variations, and chemical potential, where the results are presented graphically for proper clarity. Moreover, the particular limiting cases are also examined to validate the model and highlight key behaviors. The study is applicable in order to predict thermal and mechanical responses in electronics, MEMS/NEMS devices, aerospace components, and energy systems subjected to time-harmonic loads.

Keywords: *Dual-Phase-Lag, Fourier transform, Non-local theory, Thermoelasticity, Time Harmonic Sources*

1 INTRODUCTION

In non-local elasticity, stress at a point is affected by both the local strain and the strain distributed in the body. Non-local and lagging responses are related ideas. Non-local responses are about effects in space, and lagging responses are about delays in time. Tzou and Gao [1] built on this idea by adding nonlocal elasticity to the dual-phase-lag model first proposed by Tzou [2, 3]. This created a single framework that included both effects. At the same time, Sherief et al. [4] created a thermoelastic diffusion theory with a single relaxation time, and Sherief and Saleh [5] looked at the half-space problem in this context.

Later additions to these theories made them more general. In his work [6, 7], Sharma investigated boundary-value problems in generalized thermodiffusive elastic media and wave reflection in thermodiffusive elastic half-spaces with holes. Sharma et al. [8] looked at how viscosity affects wave propagation in Green–Naghdi type-II and type-III thermoelastic solids that are not all the same. Sharma and Marin [9] studied the reflection and transmission of plane waves at an imperfect boundary between two heat-conducting micropolar thermoelastic solids.

Sharma and Sharma [10] examined how heat sources and relaxation times affect the distribution of temperatures in living things. Marin et al. [11] looked at the Saint-Venant principle in micropolar thermoelastic diffusion when it is relaxed. Yu et al. [12] suggested a size-dependent thermoelastic model for more complex materials. This model takes into account size effects in both heat conduction and elasticity. It does this by

using generalized free energy and extended irreversible thermodynamics.

Kumar et al. [13], who looked into how deformation happens in a modified couple stress thermoelastic rotating medium when Hall current and magnetic field influences happen, using the Lord-Shulman and Green-Lindsay theories with a ramp-type thermal source. A study by Kumar et al. [14] examined a nonlocal microstretch thermoelastic thick circular plate subject to phase lags.

Sharma and Kumar [15] developed a mathematical model in photo-thermoelasticity with dual-phase lags to study deformation under concentrated inclined loads. Sharma and Khator [16, 17] addressed the challenges of renewable power generation and analyzed the planning of micro-grids for prosumers in renewable energy markets. Kumar et al. [18] looked at how non-locality and phase lags affect an MCT with mass diffusion when it was loaded in a ramp-type way.

Lotfy et al. [19] studied what happens when Hall currents and acoustic pressure are combined on nanostructured thermoelastic plates in a two-temperature, dual-phase-lag framework that is heated in a ramp-type way.

In their study, Sharma et al. [20] examined elastodynamic interactions in thermoelastic diffusion with nonlocal and phase-lag effects. Meanwhile, Marin et al. [21] used the Moore-Gibson-Thompson (MGT) heat equation to come up with a basic solution and Green's function for a semi-infinite orthotropic photo-thermoelastic medium whose properties change with temperature. They used the operator theory and the superposition principle to come up with a general solution using harmonic functions. This solution was then used to find specific solutions for steady-point heat sources at the medium's surface and within the medium.

Newer research by Alrubea and Abouelregal [22], who used the dual-phase-lag thermoelasticity model to study how nanoscale beams move when loaded by moving objects in a thermal field that decreases exponentially. Sharma et al. [23] looked into how the Moore-Gibson-Thompson equation controls thermomechanical deformation in a micropolar thermoviscoelastic solid. They found that the two-temperature effects were nonlocal and hyperbolic. In their study [24], Abouelregal et al. created a thermoviscoelastic model by combining non-local elasticity with the Kelvin-Voigt viscoelastic framework and a Klein–Gordon-type non-local elasticity formulation. They then looked at a one-dimensional half-space problem affected by an instantaneous inline heat source.

We examine how non-locality and phase lags affect thermoelastic diffusion in this study, assuming sources are distributed in a time-harmonic manner. The integral transform method is used to formulate the problem, accounting for different types of excitations, such as normal loads, thermal sources, and chemical potential sources. This formula can show how changes in size affect elastic deformation and lagging heat conduction. This makes it perfect for modeling nanoscale structures in nanotechnology applications.

2 BASIC EQUATIONS

Based on the work by Tzou & Gao [1], Sherief et al. [4], and Yu et al. [12], the equations that describe thermoelastic diffusion with dual-phase-lag and non-local effects are:

(i) Constitutive Relations

$$t_{ij} = 2\mu e_{ij} + \delta_{ij}\left[\lambda_o e_{kk} - \gamma_1 \mathrm{T} - \gamma_2 \mathrm{P}\right] \tag{1}$$

(ii) Equation of motion

$$\left(\lambda_o + \mu\right)\nabla(\nabla.\mathbf{u}) + \mu\Delta\mathbf{u} - \gamma_1\nabla\,\mathrm{T} - \gamma_2\nabla\mathrm{P} = \rho\left(1 - \xi^2\Delta\right)\frac{\partial^2 u}{\partial t^2} \tag{2}$$

(iii) Equation of heat conduction

$$\left(1 - \zeta^2\Delta + \tau_q\frac{\partial}{\partial t} + \frac{1}{2}\tau_q^2\frac{\partial^2}{\partial t^2}\right)\left(\gamma_1 T_o\dot{e} + l_1 T_o\dot{T} + T_o\dot{P}\,\mathrm{d}\right) = \mathrm{K}\left(1 + \tau_t\frac{\partial}{\partial t}\right)\Delta\mathrm{T} \tag{3}$$

(iv) Equation of mass diffusion

$$\left(1 - \zeta^2\Delta + \tau_u\frac{\partial}{\partial t} + \frac{1}{2}\tau_u^2\frac{\partial^2}{\partial t^2}\right)\left(\gamma_2\dot{e} + d\dot{T} + n\dot{P}\right) = \mathrm{D}\left(1 + \tau_p\frac{\partial}{\partial t}\right)\Delta\mathrm{P} \tag{4}$$

where

$$\lambda_o = \lambda - \beta_2^2/\mathrm{b}, \quad \gamma_1 = \beta_1 + \frac{a}{b}\beta_2, \quad \gamma_2 = \frac{\beta_2}{b}, \quad l_1 = \rho C_e/T_O + \mathrm{a}^2/\mathrm{b}, \quad \mathrm{d} = \frac{a}{b}, \quad \mathrm{n} = \frac{1}{b} \tag{5}$$

Here, u is the displacement vector, T is the temperature, P is the chemical potential, e_{ij} is the strain tensor, t_{ij} is the stress tensor, $\mu, \lambda_0, \gamma_1, \gamma_2, l_1,$ d, n, K, D are material parameters and $\tau_q, \tau_t, \tau_u, \tau_p, \xi, \zeta, \varsigma$ model parameters are defined as per the cited references.

ξ, ζ, ς are non-local parameters in equations (1)-(4). τ_q & τ_t are the thermal relaxation times with $\tau_q, \tau_t \geq 0$ and $\tau_u \& \tau_p$ are the diffusion relaxation times with $\tau_u, \tau_p \geq 0. \beta_1 = (3\lambda + 2\mu)\alpha_t, \beta_2 = (3\lambda + 2\mu)\alpha_c$. In this case, α_t, α_c are the coefficients of linear thermal expansion and diffusion expansion, respectively. Δ is the Laplacian operator, ∇ is nabla(gradient) operator. Other signs mean what they normally do.

3 PROBLEM DESCRIPTION

We consider a half-space that is uniform, isotropic, nonlocal, thermoelastic, and diffusive. This halfspace has dual-phase-lag effects and is in the region $x_3 \geq 0$. A rectangular set of Cartesian coordinates is chosen, taking (x_1, x_2, x_3) as its points of reference. The origin is placed on the boundary plane with $x_3 = 0$. The study only looks at deformations in a plane, and all the field variables are functions of (x_1, x_3, t). The half-space is loaded mechanically with a normal force, heated up, and given a chemical potential source at the boundary plane $x_3 = 0$. We assume that the variations are limited to the $x_1 - x_3$ plane for two-dimensional modeling. $u_1\,(x_1, x_3, t)$ and $u_3\,(x_1, x_3, t)$ can be written in terms of $\varphi\,(x_1, x_3, t)$ and $\psi\,(x_1, x_3, t)$ in a form that doesn't depend on the dimensions.

For two-dimensional problems, we take:

$$\begin{aligned} \mathrm{u} = (u_1\,(x_1, x_3, t)\,, 0, u_3\,(x_1, x_3, t))\,, \\ \mathrm{T}\,(x_1, x_3, t)\,, \mathrm{P}\,(x_1, x_3, t) \end{aligned} \tag{6}$$

The following equations are recovered by using (6) in (2)-(4)

$$\begin{aligned} (\lambda_o + \mu)\,\frac{\partial e}{\partial x_1} + \mu \Delta u_1 - \gamma_1 \frac{\partial\,\mathrm{T}}{\partial x_1} - \gamma_2 \frac{\partial \mathrm{P}}{\partial x_1} \\ = \rho \left(1 - \xi^2 \Delta\right) \frac{\partial^2 u_1}{\partial t^2}, \end{aligned} \tag{7}$$

$$\begin{aligned} (\lambda_o + \mu)\,\frac{\partial e}{\partial x_3} + \mu \Delta u_3 - \gamma_1 \frac{\partial\,\mathrm{T}}{\partial x_3} - \gamma_2 \frac{\partial \mathrm{P}}{\partial x_3} \\ = \rho \left(1 - \xi^2 \Delta\right) \frac{\partial^2 u_3}{\partial t^2}, \end{aligned} \tag{8}$$

$$\begin{aligned} \left(1 - \zeta^2 \Delta + \tau_q \frac{\partial}{\partial t} + \frac{1}{2}\tau_q^2 \frac{\partial^2}{\partial t^2}\right) \\ \left(\gamma_1 T_o \dot{e} + l_1 T_o \dot{T} + T_o \dot{P}\,\mathrm{d}\right) = \mathrm{K}\left(1 + \tau_t \frac{\partial}{\partial t}\right) \Delta \mathrm{T} \end{aligned} \tag{9}$$

$$\begin{aligned} \left(1 - \varsigma^2 \Delta + \tau_u \frac{\partial}{\partial t} + \frac{1}{2}\tau_u^2 \frac{\partial^2}{\partial t^2}\right) \\ \left(\gamma_2 \dot{e} + d\dot{T} + n\dot{P}\right) = \mathrm{D}\left(1 + \tau_p \frac{\partial}{\partial t}\right) \Delta \mathrm{P} \end{aligned} \tag{10}$$

The following dimensionless quantities are introduced for normalization:

$$\begin{gathered} \xi' = \frac{\omega^*}{c_1}\xi, \quad \zeta' = \frac{\omega^*}{c_1}\zeta, \quad \varsigma' = \frac{\omega^*}{c_1}\varsigma, \quad x_i' = \frac{\omega^*}{c_1}x_i, \\ u_i' = \frac{\omega^*}{c_1}u_i, \quad \mathrm{t}' = \omega^* \mathrm{t}, \quad \tau_t' = \omega^* \tau_t, \quad \tau_q' = \omega^* \tau_q, \\ \tau_u' = \omega^* \tau_u, \quad \tau_p' = \omega^* \tau_p, \quad t_{ij}' = \frac{1}{\gamma_1 T_0} t_{ij}, \\ m_{ij}' = \frac{1}{\gamma_1 T_0}\frac{\omega^*}{c_1} m_{ij}, \ \mathrm{T}' = \frac{\gamma_1}{\rho c_1^2}\,\mathrm{T}, \quad \mathrm{P}' = \frac{1}{b\gamma_2}\mathrm{P} \end{gathered} \tag{11}$$

where:

$$\omega^* = \frac{\rho C_e c_1^2}{K}, \quad c_1^2 = \frac{\lambda_o + 2\mu}{\rho}$$

Here ω^* denotes the characteristic frequency and c_1 is the longitudinal wave velocity in the medium.

Using equations (7)-(10) along with (11), and suppressing the primes, the system reduces to the following dimensionless form

$$\begin{aligned} \frac{(\lambda_o + \mu)}{\rho c_1^2}\frac{\partial e}{\partial x_1} + \frac{\mu}{\rho c_1^2}\Delta u_1 - \frac{\partial \mathrm{T}}{\partial x_1} - \frac{b\gamma_2^2}{\rho c_1^2}\frac{\partial \mathrm{P}}{\partial x_1} \\ = \left(1 - \xi^2 \Delta\right)\frac{\partial^2 u_1}{\partial t^2}, \end{aligned} \tag{12}$$

$$\begin{aligned} \frac{(\lambda_o + \mu)}{\rho c_1^2}\frac{\partial e}{\partial x_3} + \frac{\mu}{\rho c_1^2}\Delta u_3 - \frac{\partial \mathrm{T}}{\partial x_3} - \frac{b\gamma_2^2}{\rho c_1^2}\frac{\partial \mathrm{P}}{\partial x_3} \\ = \left(1 - \xi^2 \Delta\right)\frac{\partial^2 u_3}{\partial t^2}, \end{aligned} \tag{13}$$

$$\left(1-\zeta^2\Delta+\tau_q\frac{\partial}{\partial t}+\frac{1}{2}\tau_q^2\frac{\partial^2}{\partial t^2}\right)\left(\frac{\gamma_1^2}{K\rho\omega^*}T_o\dot{e}+\frac{l_1c_1^2}{K\omega^*}T_o\dot{T}+\frac{b\gamma_2\gamma_1}{K\rho\omega^*}T_o\dot{P}\,\mathrm{d}\right)=\left(1+\tau_t\frac{\partial}{\partial t}\right)\Delta\mathrm{T}, \tag{14}$$

$$\left(1-\varsigma^2\Delta+\tau_u\frac{\partial}{\partial t}+\frac{1}{2}\tau_u^2\frac{\partial^2}{\partial t^2}\right)\left(\frac{c_1^2}{Db\omega^*}\dot{e}+\frac{c_1^4d\rho}{Db\omega^*\gamma_1\gamma_2}\dot{T}+\frac{nc_1^2}{D\omega^*}\dot{P}\right)=\left(1+\tau_p\frac{\partial}{\partial t}\right)\Delta\mathrm{P} \tag{15}$$

Where:

$$\Delta=\frac{\partial^2}{\partial {x_1}^2}+\frac{\partial^2}{\partial {x_3}^2},\quad \mathrm{e}=\frac{\partial u_1}{\partial x_1}+\frac{\partial u_3}{\partial x_3}$$

4 SOLUTION PROCEDURE

The displacement components $u_1(x_1,x_3,t)$ and $u_3(x_1,x_3,t)$ can be expressed in terms of the scalar potentials $\varphi(x_1,x_3,t)$ and $\psi(x_1,x_3,t)$ in dimensionless form as:

$$u_1=\frac{\partial\varphi}{\partial x_1}-\frac{\partial\psi}{\partial x_3},\quad u_3=\frac{\partial\varphi}{\partial x_3}+\frac{\partial\psi}{\partial x_1} \tag{16}$$

Substituting (16) in equations (12)-(15), the governing system leads to the following set of coupled equations:

$$(b_1+b_2)\Delta\varphi-\mathrm{T}-b_3\mathrm{P}-\left(1-\xi^2\Delta\right)\frac{\partial^2\varphi}{\partial t^2}=0 \tag{17}$$

$$b_2\Delta\psi-\left(1-\xi^2\Delta\right)\frac{\partial^2\psi}{\partial t^2}=0 \tag{18}$$

$$\left(1-\zeta^2\Delta+\tau_q\frac{\partial}{\partial t}+\frac{1}{2}\tau_q^2\frac{\partial^2}{\partial t^2}\right)\left(b_4\Delta\dot{\varphi}+b_5\dot{T}+b_6\dot{P}\right)=\left(1+\tau_t\frac{\partial}{\partial t}\right)\Delta\mathrm{T}, \tag{19}$$

$$\left(1-\varsigma^2\Delta+\tau_u\frac{\partial}{\partial t}+\frac{1}{2}\tau_u^2\frac{\partial^2}{\partial t^2}\right)\left(b_7\Delta\dot{\varphi}+b_8\dot{T}+b_9\dot{P}\right)=\left(1+\tau_p\frac{\partial}{\partial t}\right)\Delta\mathrm{P} \tag{20}$$

Where:

$$\begin{aligned}
b_1&=\frac{(\lambda_o+\mu)}{\rho c_1^2},\quad b_2=\frac{\mu}{\rho c_1^2}\quad b_3=\frac{b\gamma_2^2}{\rho c_1^2},\\
b_4&=\frac{\gamma_1^2}{K\rho\omega^*}T_o,\quad b_5=\frac{l_1c_1^2}{K\omega^*}T_o\\
b_6&=\frac{b\gamma_2\gamma_1}{K\rho\omega^*}T_od,\quad b_7=\frac{c_1^2}{Db\omega^*},\\
b_8&=\frac{c_1^4d\rho}{Db\omega^*\gamma_1\gamma_2},\quad b_9=\frac{nc_1^2}{D\omega^*}
\end{aligned} \tag{21}$$

We assume

$$(\bar{\varphi},\bar{\psi},\bar{T},\bar{P})=(\varphi,\psi,\mathrm{T},\mathrm{P})e^{i\omega t} \tag{22}$$

We define the Fourier transform as:

$$\hat{f}(\xi_1,x_3,\omega)=\int_{-\infty}^{\infty}\bar{f}(x_1,x_3,\omega)\,e^{i\xi_1x_1}\,\mathrm{d}x_1 \tag{23}$$

By substituting equations (22) and (23) into (17)-(20) and simplifying, the system reduces to

$$\left(K_1D_1^6+K_2D_1^4+K_3D_1^2+K_4\right)(\widehat{\varphi},\widehat{T},\widehat{P})=0 \tag{24}$$

$$\left(D_1^2-m_4^2\right)\widehat{\psi}=0 \tag{25}$$

Where:

$$\begin{aligned}
K_1&=K_{11}K_{13}K_{15}-K_{33}K_{35}\zeta^2\varsigma^2K_{11}\\
&\quad+K_{31}\zeta^2K_{15}-K_{33}K_{34}\zeta^2\varsigma^2\\
&\quad-K_{31}K_{35}\zeta^2\varsigma^2b_4+K_{34}b_4K_{13}\varsigma^2\\
K_2&=K_{01}-3\xi_1^2K_1\\
K_3&=3\xi_1^4K_1-2\xi_1^2K_{01}+K_{02}\\
K_4&=K_{01}\xi_1^4-\xi_1^6K_1-\xi_1^2K_{02}-K_{03}\\
m_4^2&=\xi_1^2-\frac{\omega^2}{b_2-\xi^2\omega^2},D_1=\frac{d}{dx_3}
\end{aligned}$$

and

$$K_{01} = -K_{11}K_{22}K_{15} - K_{11}K_{13}K_{26} + K_{13}K_{15}\omega^2 + K_{33}K_{11}\zeta^2K_{25} + K_{35}\varsigma^2K_{23}K_{11} - K_{33}K_{35}\zeta^2\varsigma^2\omega^2 - K_{31}\zeta^2K_{26} - K_{21}K_{15} + K_{33}\zeta^2K_{24} + K_{34}\varsigma^2K_{23} + K_{31}\zeta^2K_{24}b_3 + K_{35}\varsigma^2K_{21}b_3 - K_{13}K_{24}b_3 - b_3K_{34}\zeta^2K_{22},$$

$$K_{02} = K_{11}K_{22}K_{26} - K_{13}K_{26}\omega^2 - K_{22}K_{15}\omega^2 - K_{11}K_{23}K_{25} + K_{33}\zeta^2K_{25}\omega^2 + K_{35}\varsigma^2K_{23}\omega^2 + K_{21}K_{26} - K_{23}K_{24} - b_3K_{21}K_{25} + b_3K_{22}K_{24}$$

$$K_{03} = \omega^2K_{26}K_{22} - \omega^2K_{23}K_{25}$$

$$K_{11} = b_1 + b_2 - \xi^2\omega^2,$$

$$K_{12} = 1 + i\omega\tau_q - \frac{\omega^2}{2}\tau_q^2,$$

$$K_{13} = b_5i\omega\zeta^2 + 1 + i\omega\tau_t, K_{14} = 1 + i\omega\tau_u - \frac{\omega^2}{2}\tau_u^2,$$

$$K_{15} = 1 + i\omega\tau_p + i\omega\zeta^2b_9, K_{21} = K_{31}K_{12},$$

$$K_{22} = K_{32}K_{12}, K_{23} = K_{33}K_{12},$$

$$K_{24} = K_{34}K_{14}, K_{25} = K_{35}K_{14}, K_{26} = K_{36}K_{14},$$

$$K_{31} = b_4i\omega, K_{32} = b_5i\omega, K_{33} = b_6i\omega,$$

$$K_{34} = b_7i\omega, K_{35} = b_8i\omega, K_{36} = b_9i\omega$$

To solve equations (24) and (25) with $\widehat{\varphi}, \widehat{\psi}, \widehat{\mathrm{T}}$ and $\widehat{P}$ disappear as x_3 approaches infinity, we write:

$$(\widehat{\varphi}, \widehat{\mathrm{T}}, \widehat{\mathrm{P}})\,(x_3, \xi_1, s) = \sum_{i=1}^{3} \left(1, R_i^*, S_i^*\right) A_i e^{-m_i x_3} \tag{26}$$

$$\widehat{\psi}\,(x_3, \xi_1, s) = A_4 e^{-m_4 x_3} \tag{27}$$

The roots of the characteristic equations (24)-(25) are $m_i (i = 1, 2, 3, 4)$ and A_i (i = 1, 2, 3, 4) are the corresponding amplitude coefficients determined from boundary conditions.

$$R_i^* = \frac{\left(m_i^2 - \xi_1^2\right)^3 \left(K_{33}K_{34}\zeta^2\varsigma^2 - K_{31}\zeta^2K_{15}\right) + \left(m_i^2 - \xi_1^2\right)^2 \left(K_{31}\zeta^2K_{26} + K_{21}K_{15} - K_{33}\zeta^2K_{24} - K_{35}\varsigma^2K_{21}\right) + \left(m_i^2 - \xi_1^2\right)(K_{21}K_{26} - K_{23}K_{24})}{\left(m_i^2 - \xi_1^2\right)^2 \left(K_{13}K_{15} - K_{33}K_{35}\zeta^2\varsigma^2\right) + \left(m_i^2 - \xi_1^2\right)\left(-K_{22}K_{15} - K_{13}K_{26} + K_{33}\zeta^2K_{25} + K_{35}\varsigma^2K_{23}\right) + (K_{22}K_{26} - K_{23}K_{25})}$$

$$S_i^* = \frac{\left(m_i^2 - \xi_1^2\right)^3 \left(K_{31}K_{35}\zeta^2\varsigma^2 - K_{34}K_{13}\varsigma^2\right) + \left(m_i^2 - \xi_1^2\right)^2 \left(K_{13}K_{24} + K_{34}\varsigma^2K_{22} - K_{31}\zeta^2K_{25} - K_{35}\varsigma^2K_{21}\right) + \left(m_i^2 - \xi_1^2\right)(K_{21}K_{25} - K_{22}K_{24})}{\left(m_i^2 - \xi_1^2\right)^2 \left(K_{13}K_{15} - K_{33}K_{35}\zeta^2\varsigma^2\right) + \left(m_i^2 - \xi_1^2\right)\left(-K_{22}K_{15} - K_{13}K_{26} + K_{33}\zeta^2K_{25} + K_{35}\varsigma^2K_{23}\right) + (K_{22}K_{26} - K_{23}K_{25})}$$

$$i = 1, 2, 3$$

5 MECHANICAL, THERMAL AND CHEMICAL POTENTIAL CONDITIONS

At the point where $x_3 = 0$, on the plane boundary, the half-space is excited from the outside by a normal mechanical load, a thermal input, and a chemical potential source. So, the boundary conditions at $x_3 = 0$ are set up to show these three types of applied fields.

$$t_{33} = -F_1(x_1)\, e^{i\omega t},$$
$$t_{31} = 0, T = F_2(x_1)\, e^{i\omega t}, \quad (28)$$
$$P = F_3(x_1)\, e^{i\omega t}$$

The non-dimensional stress components are expressed by

$$t_{33} = \frac{2\mu}{\gamma_1 T_0}\left(\frac{\partial u_3}{\partial x_3}\right) + \frac{\lambda_0}{\gamma_1 T_0}\left(\frac{\partial u_1}{\partial x_3} + \frac{\partial u_3}{\partial x_1}\right) - \frac{\rho c_1^2}{\gamma_1 T_0} T - \frac{\gamma_2^2 b}{\gamma_1 T_0}\mathrm{P} \quad (29)$$

$$t_{31} = \frac{\mu}{\gamma_1 T_0}\left(\frac{\partial u_1}{\partial x_1} + \frac{\partial u_3}{\partial x_3}\right) \quad (30)$$

Applying Fourier transform, we get

$$\hat{t}_{33} = -\hat{F}_1(\xi_1)\, e^{i\omega t}, \hat{t}_{31} = 0,$$
$$\hat{\mathrm{T}} = \hat{F}_2(\xi_1)\, e^{i\omega t}, \quad \hat{\mathrm{P}} = \hat{F}_3(\xi_1)\, e^{i\omega t} \quad (31)$$

Displacement, stress, temperature variation, and chemical potential are determined by applying equations (26) and (27) to the boundary conditions (31), taking into account equations (16), (23), (29), and (30), as follows:

$$\hat{u}_1 = -\frac{i\xi_1}{\Delta}\sum_{i=1}^{3}\Delta_i e^{-m_i x_3} + \frac{\Delta_4 m_t e^{-m_t x_3}}{\Delta} \quad (32)$$

$$\hat{u}_3 = -\frac{1}{\Delta}\sum_{i=1}^{3} m_i \Delta_i e^{-m_i x_3} - \frac{i\xi_1 \Delta_4 e^{-m_4 x_3}}{\Delta} \quad (33)$$

$$\hat{t}_{33} = \frac{1}{\Delta}\sum_{i=1}^{3} b_{1i}\Delta_i e^{-m_i x_3} + \frac{\Delta_4 b_{14} e^{-m_4 x_3}}{\Delta} \quad (34)$$

$$\hat{t}_{31} = \frac{1}{\Delta}\sum_{i=1}^{3} b_{2i}\Delta_i e^{-m_i x_3} + \frac{\Delta_4 b_{24} e^{-m_4 x_3}}{\Delta} \quad (35)$$

$$\hat{\mathrm{T}} = \frac{1}{\Delta}\sum_{i=1}^{3} R_i^* \Delta_i e^{-m_i x_3} \quad (36)$$

$$\hat{\mathrm{P}} = \frac{1}{\Delta}\sum_{i=1}^{3} S_i^* \Delta_i e^{-m_i x_3} \quad (37)$$

Here

$$\Delta = \left(S_2^* R_1^* - S_1^* R_2^*\right) n_1 + \left(S_1^* R_3^* - S_3^* R_1^*\right) n_2 + \left(S_3^* R_2^* - S_2^* R_3^*\right) n_3$$
$$n_1 = b_{13} b_{24} - b_{14} b_{23}$$
$$n_2 = b_{12} b_{24} - b_{14} b_{22}$$
$$n_3 = b_{11} b_{24} - b_{14} b_{21}$$

and

$$b_{1i} = (2r_1 + r_2) m_i^2 - \xi_1^2 r_2 - r_3 R_i^* - r_4 S_i^*,$$
$$b_{14} = 2i\xi_1 r_1 m_4,$$
$$b_{2i} = 2i\xi_1 r_1 m_i, b_{24} = -r_1\left(m_4^2 + \xi_1^2\right)$$
$$r_1 = \frac{\mu}{\gamma_1 T_0}, r_2 = \frac{\lambda_0}{\gamma_1 T_0}, r_3 = \frac{\rho c_1^2}{\gamma_1 T_0}, r_4 = \frac{\gamma_2^2 b}{\gamma_1 T_0},$$
$$i = 1, 2, 3$$

$\Delta_i (= 1, 2, 3, 4)$ are determined by changing the first, second, third, and fourth columns of Δ to

$$\left[-\hat{F}_1(\xi_1)\, e^{i\omega t}, 0, \hat{F}_2(\xi_1)\, e^{i\omega t}, \hat{F}_3(\xi_1)\, e^{i\omega t}\right]^{\mathrm{Tr}}$$

6 APPLICATIONS

6.1 Uniformly distributed source

The source is defined as:

$$[F_1(x_1), F_2(x_1), F_3(x_1)] = \begin{cases} 1 & \text{if } |x_1| \le a_0 \\ 0 & \text{if } |x_1| > a_0 \end{cases}$$

Now applying Fourier transforms to this source yields:

$$\left[\hat{F}_1(\xi_1), \hat{F}_2(\xi_1), \hat{F}_3(\xi_1)\right] = \frac{2\,\mathrm{Sin}(\xi_1 a_0)}{\xi_1}, \quad \xi_1 \neq 0 \quad (38)$$

Substituting these expressions into equations (32)-(37) provides the corresponding solutions for the field variables.

6.2 Linearly distributed source

The linearly varying source is defined as:

$$[F_1(x_1), F_2(x_1), F_3(x_1)] = \begin{cases} 1 - \frac{|x_1|}{a_0} & \text{if } |x_1| \le a_0 \\ 0 & \text{if } |x_1| > a_0 \end{cases}$$

Applying the Fourier transform at the plane boundary $x_3 = 0$in dimensionless form gives

$$\left[\hat{F}_1(\xi_1), \hat{F}_2(\xi_1), \hat{F}_3(\xi_1)\right] = \frac{2\left[1 - \cos(\xi_1 a_0)\right]}{\xi_1^2 a_0} \tag{39}$$

Here, a_0 represents the dimensionless width of the source strip. Substituting these expressions into equations (32)-(37) yields the corresponding solutions for the field variables.

7 VALIDATION

Case (I) Setting $F_2 = F_3 = 0$ in equations (32)-(37) yields the field quantities corresponding to a normal force.

Case (II) Setting $F_1 = F_3 = 0$ in equations (32)-(37) provides the corresponding quantities for a thermal source.

Case (III) Setting $F_1 = F_2 = 0$ in equations (32)-(37) gives the field quantities associated with a chemical potential source.

Subcases:

(i) Substituting $\widehat{F}_1(\xi_1), \widehat{F}_2(\xi_1), \widehat{F}_3(\xi_1)$ from equations (38) and (39) into equations (32)-(37) and incorporating case (I), produces the results for normal force (uniformly and linearly distributed).

(ii) Using the same Fourier-transformed values in equations (32)-(37) and taking case (II), provides the corresponding solutions for uniformly and linearly distributed thermal sources.

(iii) The expressions for uniformly and linearly distributed chemical potential sources are obtained by substituting the Fourier-transformed values from equations (38) and (39) into equations (32)-(37) and incorporating case (III).

Special Cases

- Setting $\xi = \zeta = \varsigma = 0$ in equations (32)-(37), invoke the case of thermoelastic diffusion described by the dual-phase-lag model.
- Setting $\tau_t = \tau_q = \tau_u = \tau_p = 0$ in equations (32)-(37) invokes the case of non-local thermoelastic diffusion.

8 INVERSION OF THE TRANSFORM

The transforms in equations (32)-(37) are inverted following the procedure outlined in [13].

9 NUMERICAL IMPLEMENTATION AND EXPLANATION

In the numerical analysis, copper is employed as the representative thermoelastic diffusion material, in line with the procedure outlined in [5].

$\lambda = 7.76 \times 10^{10}\text{Kgm}^{-1}\ \text{s}^{-2}$,
$\mu = 3.86 \times 10^{10}\text{Kgm}^{-1}\ \text{s}^{-2}, T_0 = 0.293 \times 10^3\ \text{K}$,
$C_e = 0.3891 \times 10^3\text{JKg K}^{-1}\ \text{K}^{-1}, \alpha_t = 1.78 \times 10^{-5}\ \text{K}^{-1}$,
$\alpha_c = 1.98 \times 10^{-4}\ \text{m}^3\text{Kg}^{-1}, a = 1.02 \times 10^4\ \text{m}^2\ \text{s}^{-2}\ \text{K}^{-1}$,
$b = 9 \times 10^5\text{Kg}^{-1}\ \text{m}^5\ \text{s}^{-2}, D = 0.85 \times 10^{-8}\text{Kgsm}^{-3}$,
$\rho = 8.954 \times 10^3\text{Kgm}^{-3}$, $\text{K} = 0.386 \times 10^3\text{Wm}^{-1}\ \text{K}^{-1}$,
$t = 0.01$ s, $t_0 = 0.2$ s, $\tau_t = 0.6$ s, $\tau_q = 0.7$ s,
$\tau_p = 0.8$ s, $\tau_u = 0.9$ s, $\xi = 0.395 \times 10^{-9}$ m,
$\zeta = 0.2 \times 10^{-9}$ m, $\varsigma = 0.15 \times 10^{-9}$ m

MATLAB (R2016a) was used to carry out numerical simulations that evaluate normal stress, tangential stress, tangential couple stress, temperature changes, and chemical potential under the following conditions:

1. Thermoelastic diffusion incorporating both non-local effects and dual-phase-lag.
2. Dual-phase-lag thermoelastic diffusion without non-local effects.
3. Non-local thermoelastic diffusion without diffusion phase-lags.

4. Non-local thermoelastic diffusion without thermal phase-lags.

5. Non-local thermoelastic diffusion with no phase-lags.

Figures 1-9 correspond to uniformly distributed normal forces, while Figures 10-18 represent linearly distributed forces.

- Figures 1-3 and 10 -12 present the influence of normal loading for all cases, considering both uniformly and linearly distributed forces.
- Figures 4-6 and 13-15 show the impact of thermal sources for all cases, again under uniformly and linearly distributed forces.
- Figures 7-9 and 16-18 show the influence of chemical potential sources for all cases under uniformly and linearly distributed forces, respectively.

In all figures:

- Solid line (___) represents thermoelastic diffusion with non-local effects and dual-phase-lag (TNP).
- Small dashed line (- - -) denotes thermoelastic diffusion with dual-phase-lag but without non-local effects (WNTP).
- Large dashed line (__ __) corresponds to non-local thermoelastic diffusion without diffusion phase-lag (TNWDP).
- Solid line with central marker (-*-) indicates non-local thermoelastic diffusion without thermal phase-lag (TNWTP).
- Large dashed line with central marker (-o-) represents non-local thermoelastic diffusion without any phase-lags (TN).

9.1 Normal load (uniformly distributed sources)

Figure 1 illustrates the distribution of t_{33} vs x_1. The magnitude of t_{33} decreases monotonically within the bounded region near the load application, which reflects the expected relaxation of normal stress due to the direct action of the applied normal load. Beyond this bounded zone, however, t_{33} shows a reversal trend and increases gradually as x_1 grows. Such a trend is characteristic of the model where stress effects are not confined locally but spread spatially due to size-dependent interactions.

Figure 2 depicts the thermal response T across the coordinate x_1. For all considered cases, the temperature magnitude decreases consistently as x_1 increases. This uniform reduction highlights the dissipative nature of heat transfer in the medium under the DPL framework. A noteworthy observation is that the decay profile of T is nearly identical in the WNTP (Without Non-thermal Potential) and TN (Thermal Nonlocality) cases.

The variation of the chemical potential P is presented in Figure 3. For all scenarios, P decreases steadily with increasing x_1. This trend signifies a gradual diffusion of chemical potential away from the loaded boundary. Moreover, the decrement pattern of P is nearly uniform across all cases under normal loading.

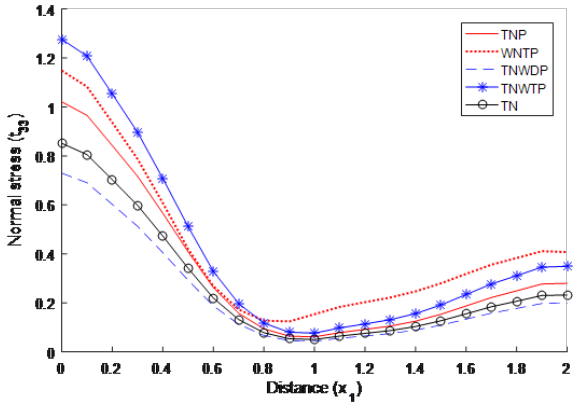

Fig. 1 Evolution of t_{33} profile vs x_1

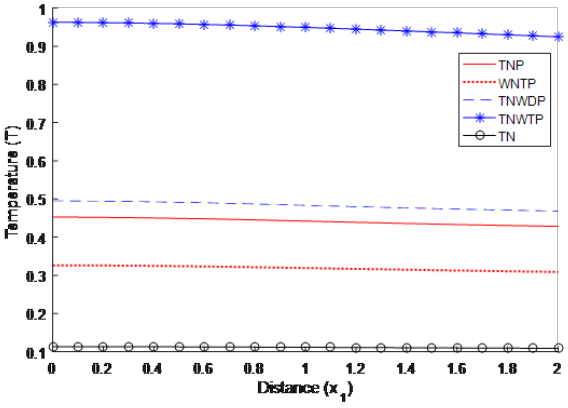

Fig. 2 Evolution of T profile vs x_1

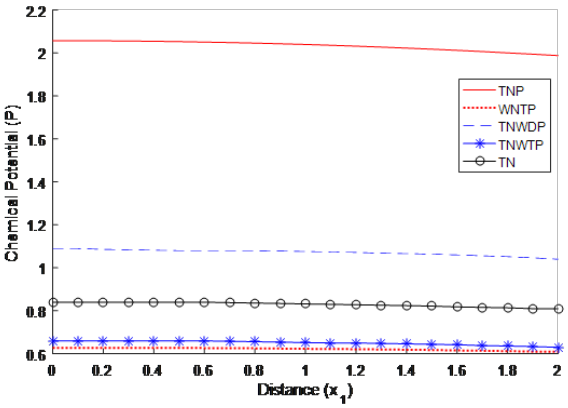

Fig. 3 Evolution of P profile vs x_1

9.2 Thermal load (uniformly distributed sources)

Figure 4 shows the distribution of t_{33} along the horizontal axis x_1 . Initially, t_{33} decreases sharply near the source, indicating rapid relaxation of stress generated by thermal expansion in the immediate vicinity of the heating zone. Beyond this region, stress does not simply decay but exhibits oscillatory behavior for all cases. The delayed heat conduction (due to phase lags) introduces a wave-like effect into the stress distribution, while non-locality ensures that stress influence extends beyond the direct loading zone, producing the observed oscillations.

Figure 5 presents the thermal field T along the x_1-axis under thermal loading. Across all cases, the temperature field T decreases monotonically as x_1 increases, showing a consistent thermal diffusion profile. The decrement is gradual rather than abrupt, which reflects the joint influence of non-local heat conduction and the DPL model. Non-locality ensures that the temperature field T extends beyond the immediate heated boundary, while phase lags introduce a delayed heat-transfer mechanism, resulting in smoother attenuation rather than steep gradients.

Figure 6 depicts the variant of P along the x_1-axis. A striking difference is observed among the cases: for TNWDP, P increases monotonically with distance. Conversely, for all other cases (TNP, WNTP, TNWTP, and TN), the magnitude of P decreases monotonically, consistent with the expected diffusion-driven relaxation pattern in which the chemical potential P gradually dissipates away from the source.

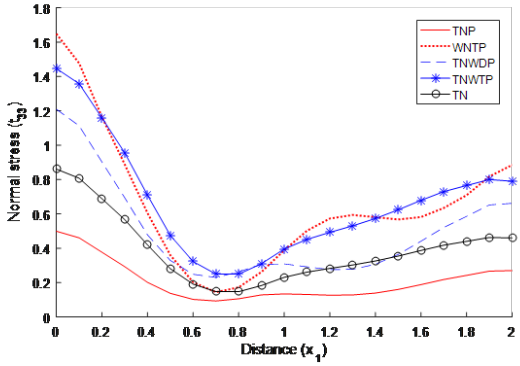

Fig. 4 Distance-dependent profile of normal stress

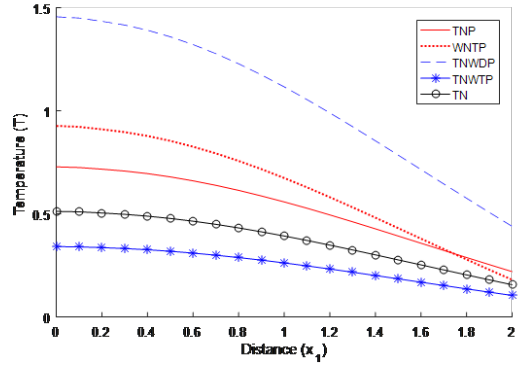

Fig. 5 Distance-dependent profile of temperature.

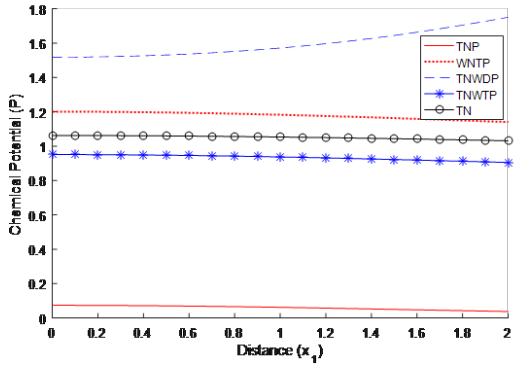

Fig. 6 Distance-dependent profile of chemical potential

9.3 Chemical potential (uniformly distributed sources)

Figure 7 presents the variant of t_{33} vs x_1. Close to the source, t_{33} decreases rapidly, indicating stress relaxation in the immediate vicinity of the applied excitation. Beyond this region, however, the stress exhibits oscillatory behavior for all the considered cases. The oscillations reflect the effects (non-local and phase-lag), which allow the stress to propagate in a wave-like manner rather than decaying monotonically. Among all cases, the oscillatory amplitude for WNTP is notably larger.

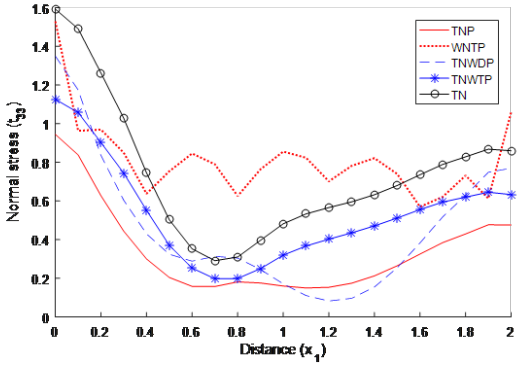

Fig. 7 Distribution of t_{33} vs x_1

Figure 8 illustrates the thermal field T as a function of x_1. For all cases, the temperature diminishes monotonically with increasing $x_1$from the boundary. The decrement is smooth and nearly identical across the different cases, which shows that the thermal response under chemical excitation is weakly affected by variations in the non-local and phase-lag parameters. This uniform attenuation suggests that, unlike mechanical stresses, the thermal field remains relatively insensitive to the precise formulation of the lagging and non-locality assumptions when driven by chemical potential sources.

The variant of P is displayed in Figure 9. For all models considered, P decreases steadily with increasing x_1. The decline is gradual rather than abrupt, reflecting the diffusive transport of chemical potential away from the source. The similarity of this trend across all cases indicates that, unlike shear and normal stresses, chemical potential diffusion is robust and affected by changes in non-local elasticity or phase-lag formulations

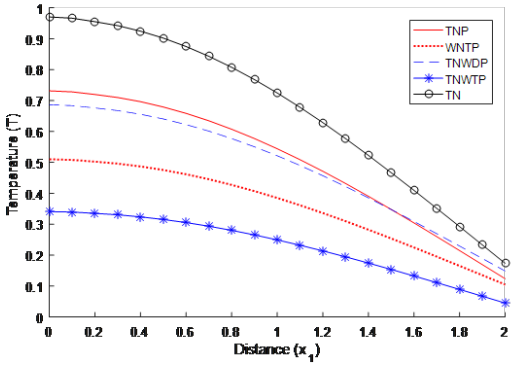

Fig. 8 Distribution of T vs x_1

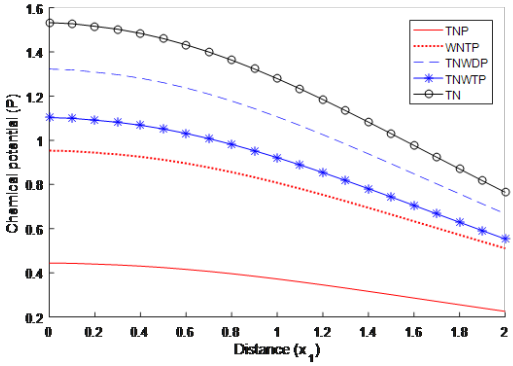

Fig. 9 Distribution of P vs x_1

9.4 Normal load (linearly distributed sources)

Figure 10 displays the distribution of t_{33} when the boundary is subjected to a normal load. Near the loading zone, t_{33} decreases in magnitude, reflecting stress release in the immediate vicinity of the applied force. Beyond this region, the stress response becomes oscillatory for all the cases considered. Interestingly, the oscillation patterns are nearly identical in amplitude and frequency across all cases. This indicates a strong dominance of the applied mechanical source over model-specific parameters.

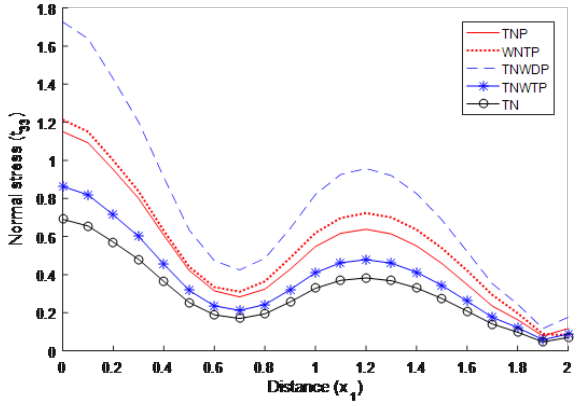

Fig. 10 Distance-dependent normal stress distribution

Figure 11 describes T with x_1. In all cases, the temperature decreases monotonically with distance from the boundary, indicating a consistent thermal diffusion process. The rate of decrease is almost identical across all models, suggesting that under normal loading, the thermal response is influenced by the presence or absence of non-local or phase-lag effects.

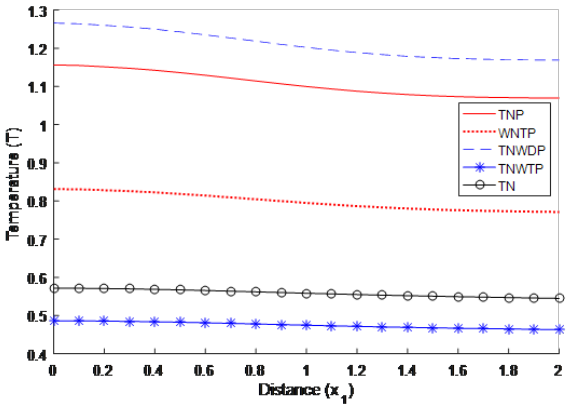

Fig. 11 Distance-dependent temperature change distribution

The chemical potential P, shown in Figure 12, also decreases steadily with increasing x_1 for all cases. The trend is smooth and nearly identical across cases, reflecting uniform diffusion of chemical potential away from the loaded boundary. The fact that the decrement is the same across all models indicates that, similar to the thermal field, chemical potential diffusion under normal loading is affected by variations in non-local elasticity and phase-lag formulations.

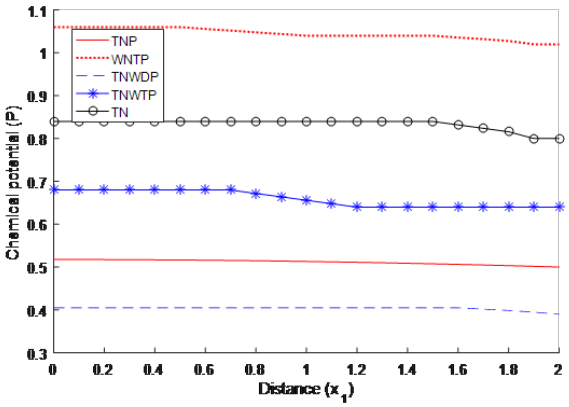

Fig. 12 Distance-dependent chemical potential distribution

9.5 Thermal source (linearly distributed sources)

Figure 13 presents the revamping of t_{33} along the x_1-axis under thermal loading. Close to the source, t_{33} decreases sharply, showing the immediate stress relaxation due to localized thermal expansion. Inside the bounded region, however, t_{33} increases, which

indicates stress redistribution caused by the delayed thermal response under the DPL framework. Beyond this zone, t_{33} again decreases for all considered cases, confirming that the stress eventually dissipates away from the source application

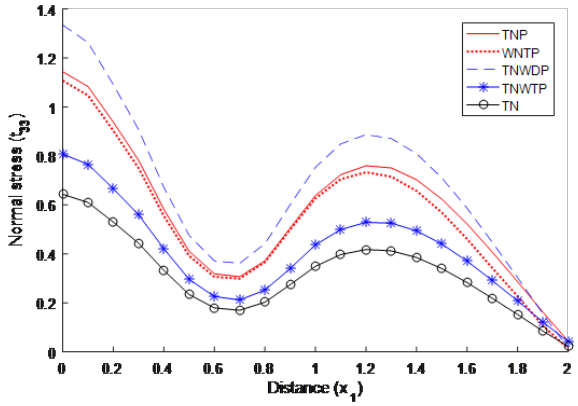

Fig. 13 Distance-dependent profile of normal stress

Figure 14 illustrates the thermal field T along the x_1-axis. For all cases, T decreases gradually as x_1 increases. The decay is smooth and nearly identical across models, which indicates that the overall temperature attenuation under thermal excitation is stable and consistent.

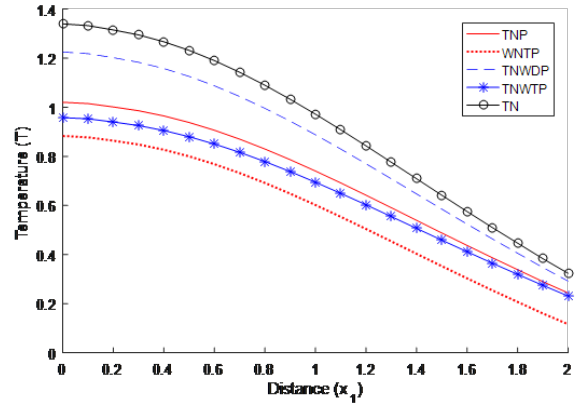

Fig. 14 Distance-dependent profile of temperature change

Figure 15 displays the distribution of chemical potential P. The response varies distinctly between the cases: for TNWDP, P increases with distance, indicating a buildup of chemical potential caused by the dual-phase-lag effect delaying diffusion. For TNP, P decreases initially within the bounded region but then increases again, reflecting a non-monotonic redistribution of chemical potential. In contrast, for WNTP, TNWTP, and TN, P decreases gradually for all values of x_1.

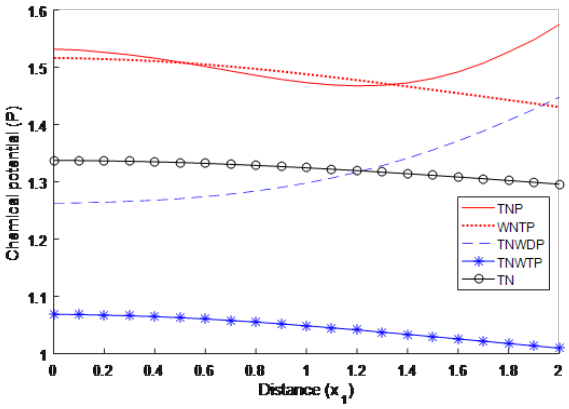

Fig. 15 Distance-dependent profile of chemical potential

9.6 Chemical potential source (linearly distributed sources)

Figure 16 illustrates the response of the normal stress t_{33} when the boundary is excited by a chemical potential source. Close to the application point, t_{33} decreases, indicating stress relaxation near the boundary. Within the bounded region, the stress shows a reversal and increases before gradually decreasing again at larger distances. This non-monotonic pattern demonstrates the redistribution of stresses due to the coupling between chemical diffusion and mechanical deformation, with the dual-phase-lag effect contributing to delayed stress responses beyond the loading zone.

Figure 17 presents the temperature distribution T along the horizontal axis. For all cases, T decreases monotonically as distance increases, reflecting the expected thermal relaxation behavior. The trends are nearly identical across all cases, showing that thermal response under chemical excitation is significantly influenced by variations in the non-local or phase-lag formulations

The variation of chemical potential P is shown in Figure 18. Across all cases, P decreases gradually

with increasing x_1, showing a smooth and monotonic decline. This indicates that chemical diffusion remains the dominant mechanism, leading to steady dissipation of concentration gradients away from the boundary. The similarity in trends across all cases indicates that, under chemical excitation, the chemical potential field is robust and depends on non-local and phase-lag variations.

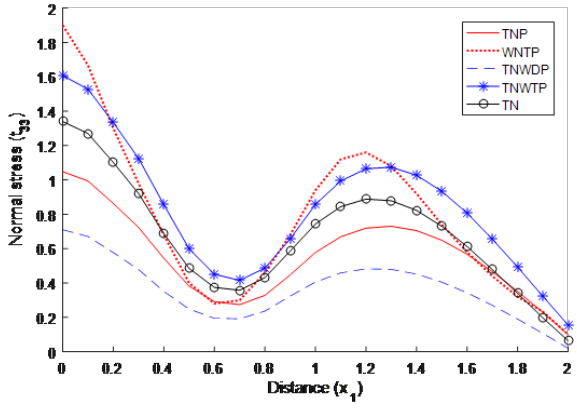

Fig. 16 Evolution of normal stress profile with distance

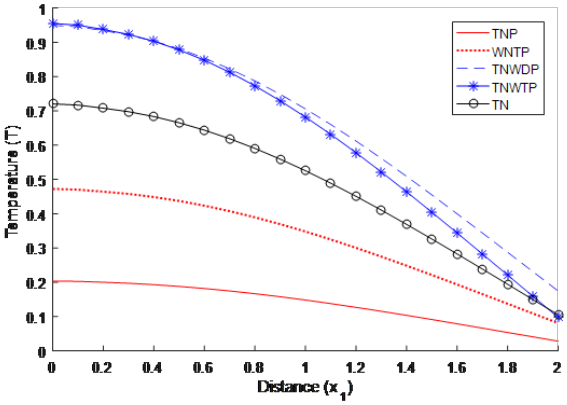

Fig. 17 Evolution of temperature change profile with distance

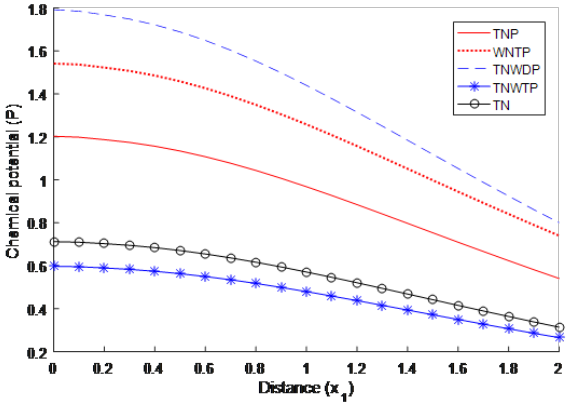

Fig. 18 Evolution of chemical potential profile with distance

10 CONCLUSION

This study investigates the combined effects of non-locality and phase-lag phenomena in a modified couple stress thermoelastic half-space exposed to thermomechanical loading. The mathematical model was developed and solved using integral transform methods. Two categories of external excitations were examined: uniformly distributed sources and linearly varying sources.

For a uniformly distributed mechanical load, the normal stress component displayed oscillatory characteristics, while both temperature and chemical potential diminished progressively with distance from the source. In the case of a uniformly distributed thermal load, oscillations appeared in the stress component, whereas the temperature and chemical potential fields consistently decreased in magnitude. Likewise, when a uniformly distributed chemical potential source was applied, the stress component revealed distinct oscillations, but the associated temperature and chemical potential distributions decayed smoothly with distance.

For linearly distributed normal loading, normal stress and chemical potential decreased in magnitude, while the temperature field displayed oscillatory fluctuations. Linearly distributed thermal loading produced inconsistent and non-uniform patterns in the resulting fields, while linearly distributed chemical potential loading led to oscillatory trends at larger distances from the source.

The problem finds applications in semiconductor technologies, thermal barrier coatings, and composite materials due to coupled thermo-diffusive loading. Furthermore, the results are useful in biomechanics and nanotechnology.

Acknowledgement

N/A

Funding source

No funds received.

Data availability

N/A

DECLARATIONS

Conflict of interest

The authors declare no competing interests.

Consent to publish

N/A

Ethical approval

N/A

REFERENCES

[1] Tzou DY, Guo ZY. Nonlocal behavior in thermal lagging. International Journal of Thermal Sciences. 2010;49(7):1133–1137. 10.1016/j.ijthermalsci.2010.01.022

[2] Tzou DY. A Unified Field Approach for Heat Conduction From Macro- to Micro-Scales. Journal of Heat Transfer. 1995;117(1):8–16. 10.1115/1.2822329

[3] Tzou DY. The generalized lagging response in small-scale and high-rate heating. International Journal of Heat and Mass Transfer. 1995;38(17):3231–3240. 10.1016/0017-9310(95)00052-b

[4] Sherief HH, Hamza FA, Saleh HA. The theory of generalized thermoelastic diffusion. International Journal of Engineering Science. 2004;42(5–6):591–608. 10.1016/j.ijengsci.2003.05.001

[5] Sherief HH, Saleh HA. A half-space problem in the theory of generalized thermoelastic diffusion. International Journal of Solids and Structures. 2005;42(15):4484–4493. 10.1016/j.ijsolstr.2005.01.001

[6] Sharma K. Boundary value problems in generalized thermodiffusive elastic medium. Journal of Solid Mechanics. 2010;2(5):348-62

[7] Sharma K. Reflection of plane waves in thermodiffusive elastic half-space with voids. Multidiscipline Modeling in Materials and Structures. 2012;8(3):269–296. 10.1108/15736101211269113

[8] Sharma S, Sharma K, Bhargava RR. Effect of viscosity on wave propagation in anisotropic thermoelastic with Green-Naghdi theory type-II and type-III. Mater Phys Mech. 2013;16(2):144-58

[9] Sharma K, Marin M. Reflection and transmission of waves from imperfect boundary between two heat conducting micropolar thermoelastic solids. Analele Universitatii "Ovidius" Constanta - Seria Matematica. 2014;22(2):151–176. 10.2478/auom-2014-0040

[10] Sharma S, Sharma K. Influence of Heat Sources and Relaxation Time on Temperature Distribution in Tissues. International Journal of Applied Mechanics and Engineering. 2014;19(2):427–433. 10.2478/ijame-2014-0029

[11] Marin M, Abbas I, Kumar R. Relaxed Saint-Venant principle for thermoelastic micropolar diffusion. Struct Eng Mech. 2014;51(4):651-62

[12] Yu YJ, Tian XG, Xiong QL. Nonlocal thermoelasticity based on nonlocal heat conduction and nonlocal elasticity. European Journal of Mechanics - A/Solids. 2016;60:238–253. 10.1016/j.euromechsol.2016.08.004

[13] Kumar R, Devi S, Sharma V. Effects of Hall Current and Rotation in Modified Couple Stress Generalized Thermoelastic Half Space due to Ramp-Type Heating. Journal of Solid Mechanics. 2017;9(4):527-42

[14] Kumar R, Miglani A, Rani R. Transient analysis of nonolocal microstretch thermoelastic thick circular plate with phase lags. Med J Model Simul. 2018;9:25-42

[15] Sharma N, Kumar R. Photothermoelastic deformation in dual phase lag model due to concentrated inclined load. Ital J Pure Appl Math. 2022;48:1147-60

[16] Sharma S, Khator S. Power generation planning with reserve dispatch and weather uncertainties including penetration of renewable sources. International Journal of Smart Grid and Clean Energy. 2021:292–303. 10.12720/sgce.10.4.292-303

[17] Sharma S, Khator S. Micro-Grid Planning with Aggregator's Role in the Renewable Inclusive Prosumer Market. Journal of Power and Energy Engineering. 2022;10(04):47–62. 10.4236/jpee.2022.104004

[18] Kumar R, Kaushal S, Dahiya V. Response of Non-Local and Phase-Lags due to Ramp-Type Loading in Modified Couple Stress Thermoelastic with Mass Diffusion. Mechanics of Solids. 2021;56(4):559–570. 10.3103/s0025654421040117

[19] Lotfy K, Elshazly IS, Halouani B, Sharma S, Ailawalia P, El-Bary AA. Influence of Hall current and acoustic pressure on nanostructured DPL thermoelastic plates under ramp heating in a double-temperature model. Open Physics. 2025;23(1). 10.1515/phys-2025-0125

[20] Sharma S, Marin M, Altenbach H. Elastodynamic interactions in thermoelastic diffusion including non-local and phase lags. ZAMM - Journal of Applied Mathematics and Mechanics / Zeitschrift für Angewandte Mathematik und Mechanik. 2025;105(1). 10.1002/zamm.202401059

[21] Marin M, Sharma S, Kumar R, Vlase S. Fundamental solution and Green's function in orthotropic photothermoelastic media with temperature-dependent properties under the Moore–Gibson–Thompson model. ZAMM - Journal of Applied Mathematics and Mechanics / Zeitschrift fur Angewandte Mathematik und Mechanik. 2025;105(6). 10.1002/zamm.70124

[22] Alrubea NA, Abouelregal AE. Analyzing nanoscale beam dynamics under moving loads and thermal decay with a DPL Thermoelastic Framework. Results in Engineering. 2025;26:105316. 10.1016/j.rineng.2025.105316

[23] Sharma K, Marin M, Kumar R. Thermomechanical deformation in a micropolar thermoviscoelastic solid under the Moore-Gibson-Thompson heat equation with nonlocal and hyperbolic two-temperature effects. Journal of Computational Applied Mechanics. 2025;56(4):720-36

[24] Abouelregal AE, Marin M, Alhassan Y, Atta D. A Novel Space–Time Nonlocal Thermo-Viscoelastic Model with Two-Phase Lags for Analyzing Heat Diffusion in a Half-Space Subjected to a Heat Source. Iranian Journal of Science and Technology, Transactions of Mechanical Engineering. 2025;49(3):1315–1332. 10.1007/s40997-025-00835-9

How to cite this article

Kumar R, Kumari P, Menaka. Thermoelastic Diffusion with Dual-Phase-Lag: Analysis of Time-Harmonic Sources in a Non-Local Framework. Journal of University of Anbar for Pure Science. 2026; 20(1):322-336. doi:10.37652/juaps.2025.165066.1681